GEOFIZIKA VOL. 31 2014

DOI: 10.15233/gfz.2014.31.5
Original scientific paper
UDC: 551.555.4

The role of advection and of work done by forces in the gustiness of the Bora flow

Jože Rakovec [1], *Rahela Žabkar* [1] *and Mark Žagar* [2]

[1] University of Ljubljana, Faculty of Mathematics and Physics, Ljubljana, Slovenia and Slovenian Centre of Excellence for Space Sciences and Technologies, Ljubljana, Slovenia

[2] Vestas Wind Systems, Aarhus, Denmark

Received 15 May 2014, in final form 27 August 2014

Local wind changes within the flow of the Adriatic Bora are investigated in the case of 8 December 2001 that was simulated with the WRF/ARW model in a 333 m horizontal resolution and with all relevant model variables archived during a 3 h time interval with 1 s temporal resolution. Along a selected cross section, two locations of strong gusts in the lee of a Dinaric mountain ridge are found – the upper one on the slope and the other over the sea close to the coastline; in between the wind is considerably weaker. About 16 to 18 gusts developed in the 3 h interval at both locations with an average period of approximately 8.5 min. The advective transport of kinetic energy (*KE*), the work of the unbalanced part of the pressure gradient force and the diffusion and dissipation of *KE* cause the local change ΔKE, and their quasi-periodic fluctuations lead to gusts and lulls. The results of the numerical simulation enable an estimation of the contributions of advection, the work of forces and of turbulence and dissipation effects. Advective contributions to local changes are more or less in the phase with ΔKE and ahead of the phase of *KE*, while the contributions of work are generally smaller and in the opposite phase: so in general the advection and the work effects oppose each other. The advection and the work effects are not spatially homogeneous, i.e. they cease and even change their sign between the two locations of the strongest gusts and so there is no continuous displacement of *KE* from the upper to the lower location by either of the two effects: their contributions interchange with each other down the slope.

Keywords: bora gustiness, internal flow dynamics, WRF-ARW model

1. Introduction

The Bora is a north-easterly wind (from the Greek *Boreas* – northern) that blows into the Adriatic basin. Winds of the same type and structure also appear elsewhere in the world. The main characteristic of the Adriatic Bora is the invasion of cold air into the Pannonian basin and its acceleration after crossing the

mountains that run alongside the Adriatic basin. The traditional explanation (AMS Glossary) was that the Bora is "a fall wind with a source so cold that, when the air reaches the lowlands or coast, the dynamic warming is insufficient to raise the air temperature to the normal level for the region". This dynamic explanation of the Bora was revised after an intensive measurement campaign in ALPEX (Smith, 1987), numerical modelling (e.g. Klemp and Durran, 1987), and additional conceptual models (e.g. Smith and Sun, 1987). Some recent studies reveal that certain instances of Bora exhibit a downslope windstorm or hydraulic jump structure (AMS Glossary). A comprehensive review of Bora characteristics was recently published by Grisogono and Belušić (2009).

It has long been known that gustiness is one of the Bora's chief characteristics. A few decades ago, the spectrum of gusts in the Adriatic Bora was measured (Rakovec, 1987) and several authors (e.g. Yoshino, 1976; Petkovšek 1982, 1987) attempted to explain it by the quasi-periodic spills of cold air masses over the mountain ridge. More recent investigations associate the gustiness with the upper-tropospheric jet and tropopause behaviour, e.g. Belušić et al. (2004, 2007). Their results suggest that Kelvin-Helmholtz instability (KHI) is the most likely pulsating mechanism (Grisogono and Belušić, 2009). This instability appears above the Bora shooting flow, which is essentially a jet with a maximum of about 300 – 500 m AGL, and below the wave-breaking region. They further showed that the enhanced positive vertical wind shear induced by the passage of the upper tropospheric jet stream weakened the primary (i.e. low-level) wave breaking in the lower troposphere. This decrease of non-linearity occurs because the local non-linearity measure $NLM = N(z)h / u(z)$ (Durran, 2003; Jiang and Smith, 2003); where $N(z)$ is the Brunt-Väisäla frequency, h is the mountain height, and $u(z)$ is the wind velocity) decreases with an increase in the mean wind speed; instead of the primary wave breaking, large lee waves occur. After the vertical shear above the Bora jet diminished, the KHI was suppressed and hence the related pulsations disappeared. This whole explanation is thus based on a consideration of the processes occurring above the Bora shooting flow.

Apart from the explanations for gustiness based on external conditions out of the flow, it might be interesting to investigate the internal flow dynamics. In the present paper we therefore focus on the internal structure and near-surface energetics of the downslope flow, especially on the local contribution of advection and of the local work of forces to local changes of kinetic energy in a flow: we are interested in ascertaining how the high kinetic energy (*KE*) accumulates in the gusts at these locations: what is the contribution of advection, what is that of the work of forces and what is the role of turbulent diffusion and energy dissipation.

2. The methodology

The conservation principle may be expressed in different formulations. One of these is a transport or balance equation which states that locally a change in

a certain quantity is caused by the divergence of the transport of that quantity, and by sources or sinks of that quantity. Transport equations for atmospheric $KE \equiv \rho v^2/2$ can be derived by multiplying the equation of motion with $\rho\vec{v}$ to obtain $\rho\vec{v}\frac{d\vec{v}}{dt} = \rho\frac{d}{dt}\left(\frac{v^2}{2}\right) = -\vec{v}\cdot\nabla p + \rho\vec{v}\cdot\vec{g} + \rho\vec{v}\cdot\vec{f}$ and by multiplying the continuity equation with $\frac{v^2}{2}$ resulting in $\frac{v^2}{2}\frac{d\rho}{dt} = -\frac{v^2}{2}\rho\nabla\cdot\vec{v}$. The summation of both equations results in an equation for the balance of *KE* (see, for example, Van Migheim, 1973):

$$\frac{\partial KE}{\partial t} = -\nabla\cdot\left(KE\vec{v}\right) - \vec{v}\cdot\nabla p + \rho\vec{v}\cdot\vec{g} + \rho\vec{v}\cdot\vec{f} \tag{1}$$

After splitting the pressure into the hydrostatic and non-hydrostatic parts in Eq. (1), the gravity effects completely cancel the effects of the hydrostatic part of the vertical pressure gradient force. In such a simplified form, the advection $Adv = -\nabla\cdot\left(KE\vec{v}\right)$, the work done by the remaining forces $Wrk = \left(-w\frac{\partial p_{nh}}{\partial z} - \vec{v}_h\cdot\nabla_h p\right)$, and the turbulent diffusion and energy dissipation $Turb = \rho\vec{v}\cdot\vec{f}$ contribute to the local changes of *KE:*

$$\frac{\partial\left(KE\right)}{\partial \mathrm{t}} \equiv \Delta KE = Adv + Wrk + Turb = -\nabla\cdot\left(KE\vec{v}\right) + \left(-w\frac{\partial p_{nh}}{\partial z} - \vec{v}_h\cdot\nabla_h p\right) + \rho\vec{v}\cdot\vec{f} \tag{2}$$

More details on the applied methodology are given in Appendix A. Here we mention only that a great part of the vertical gradient force balances with gravity and so only the non-hydrostatic part of the gradient force acts along a vertical direction, altogether with the complete gradient force along a horizontal direction (the two terms in parentheses).

A somewhat similar diagnosing approach was used by e.g. Poulos et al. (2007), except for velocity and not KE when investigating the flow in the Eldorado Canyon in Colorado. They thus had to consider more terms: advection, pressure gradient, gravity, Coriolis effects, and turbulent momentum flux contributing to local changes in wind velocity. Moreover, periodic oscillations were essentially absent in their case, while in the case of the Bora strong oscillations with a periodicity of around 8.5 min are the primary object of examination.

3. The diagnostic sub-domain and the data

The case of the Bora on 8 December 2001 over part of the Dinaric Alps in the lee of the Velebit mountain ridge with strong pulsations was simulated using WRF-ARW, version 3.2.1 (Skamarock et al., 2008). The region is one of the best known areas of strong and pulsating Bora and has a measuring station at Senj

on the coastline – see Fig. 1. Another area further to the north of strong Bora is in the lee of the Dinaric-Alpine ridges across the Vipava valley, Karst and Trieste, and to the south there are areas of strong Bora in Dalmatia in the lee of the Dinaric mountain ridges of Mosor and Biokovo. The same case had already been investigated by Belušić et al. (2007). The model was configured with two-way nesting from a 27 km down to a 1 km resolution in a ratio of 3, followed by the fourth nesting of a domain with a 333 m horizontal resolution and 181 × 181 grid points in the horizontal – it is shown in Fig. 1. In all domains the model has 62 vertical levels extending up to 50 hPa so the lowest few levels near the surface are at about 16, 54, 138 m, etc. ECMWF operational analyses were used for the initial and lateral boundary conditions. The simulation in the third 1 km resolution domain started at 12 UTC and ended at 18 UTC, while in the smallest 333 m resolution domain it started at 14 UTC and ended at 18 UTC. In the nested domain, a Smagorinsky 3-D first-order closure was used for turbulence and mixing. Since in our specific case this parameterisation alone did not produce the proper vertical wind profile (the wind was strongest at the surface), and did not produce the hydraulic jump-like structure, the Janjić (Eta) version of Monin-

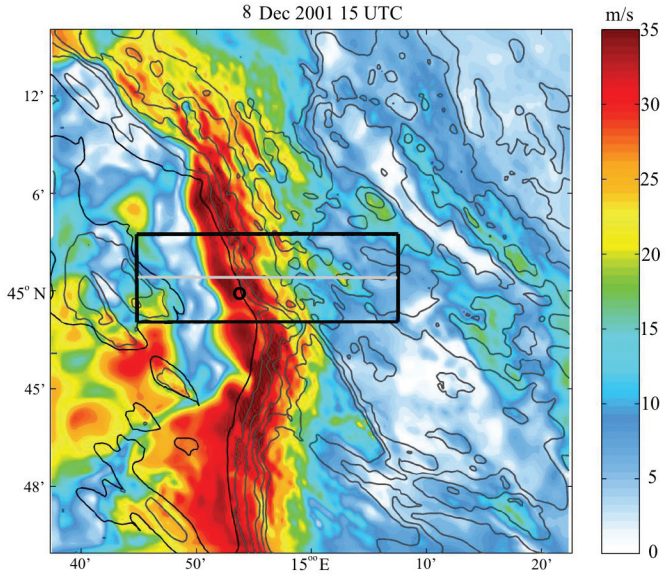

Figure 1. Horizontal cross-section of wind velocity (in m s^{-1}) on model level 2 (over the sea at a height of approximately 54 m) for 8 Dec 2001 at 15 UTC in the nested domain with a 333 m resolution. A black rectangle marks the sub-domain of the detailed analysis of approximately 30 km × 10 km horizontally (90 × 30 grid-points), the light grey central line in the middle of rectangle indicates the position of the vertical cross-sections ($Y = 14$), and the black circle the location of the wind measurements at Senj. The thin black line is the coastline, while the dark grey lines represent the relief contours with a 200 m interval.

Obukhov surface layer physics, and the Mellor-Yamada-Janjić (Eta) boundary layer parameterisation were also used. This involves some sort of 'double counting' of turbulence but produces results that are closer to the experimental evidence than without it.

We focus on events inside the sub-domain (the black rectangle in Fig. 1) between 15:10 and 18:00 UTC when around 16 to 18 gusts developed there. In this smaller sub-domain of the detailed analysis with 90 grid points along X and 30 grid points along Y and with 62 levels in the vertical, all of the main model's variables (three wind components, temperature, density, pressure, geopotential) were archived every second. These values were smoothed in time with a 7-time-point moving averages operator (selected quite arbitrarily, without a physical reason; some more or less smoothing points would not cause an essentially different result):

$$\overline{\chi}(t) = \left[\chi(t-3\Delta t) + 2\chi(t-2\Delta t) + 3\chi(t-\Delta t) + 3\chi(t) + 3\chi(t+\Delta t) + 2\chi(t+2\Delta t) + \chi(t+3\Delta t)\right]/15.$$

From such smoothed values the terms $KE, \Delta KE$, Adv, Wrk, and $Turb$ were calculated according to their definitions in Section 2. It should be mentioned that the terms being computed as finite differences are burdened by some errors, for example errors arising from the interpolation of wind variables during de-staggering, errors of computing the pressure gradient in a σ coordinate system etc.

4. Low-level flow analysis

4.1. Some general spatial characteristics

The simulation results reveal a two-layer structure of the flow in the lower troposphere (Fig. 2). The lowest, very stable layer is roughly 3 km deep on the upstream side of the mountain and about 1 km deep downslope the mountain ridge. A strong low-level jet (LLJ) – a jet from E to W ($u < 0$) – stays attached to the surface along the slope and above the sea until about 5.5 km from the coast where there is a more or less stationary position of a jump of the flow rising to 1.5 km, occasionally even 3 km in height. When considering the structure of the Bora it is also worthwhile paying attention to the reverse flow above the main low-level jet (Fig. 2). The reverse flow is present most of the time above the Bora LLJ. When the flow thins into a jet of highest velocities the layer of reverse flow descends. There is a reverse flow also in a part of a rotor below the jump.

The upstream velocity u is small compared to the velocity inside the Bora LLJ, approximately 15 m s^{-1}. A wavy structure with a horizontal wavelength of $\lambda_x \approx 8$ km can be observed on the upwind side of the mountain. The flow becomes shallower as it approaches the ridge and is about 1 km deep just above the steepest slope, and thins further to a depth of about 800 m over the sea. The depth varies in time. The flow accelerates to about 30 m s^{-1} at the ridge and up to 45 m s^{-1} in gusts over the slope and over the foothills. The upstream Brunt-

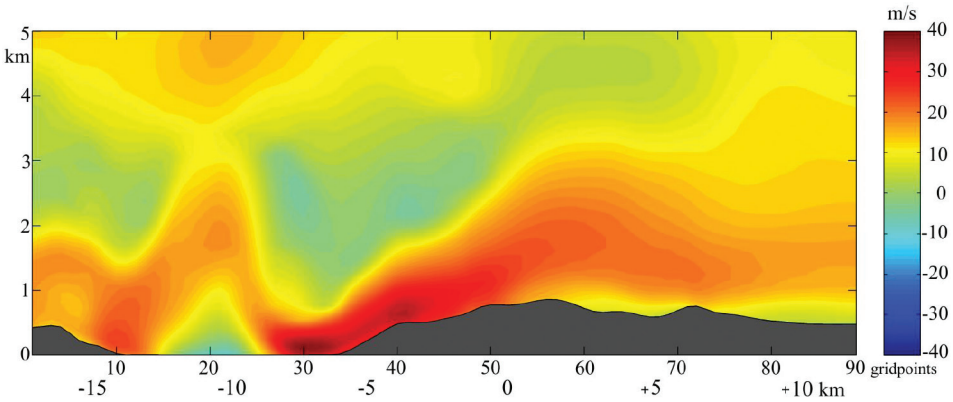

Figure 2. Vertical cross-section of the westward wind component (–*u*) along the middle of the sub-domain rectangle at 15 UTC. Westward directed bora flow (red hues) thinning from the windward side into a strong bora low-level jet (LLJ) and eastward directed reverse flow above the main bora LLJ (blue hues) are presented. Note the wavy structure on the upwind side of the mountain and the flow jump over the sea some 5.5 km away from the coastline.

Väisäla frequency N for the whole troposphere is around 0.014 s^{-1}, while the lowest 1500 m are more stable with $N = 0.017$ s^{-1}. For this case, Belušić et al. (2007) estimated the local nonlinearity measure in the upstream flow $NLM = N(z)h / u(z)$ to be greater than 1 in the lowest 5 km during the pulsations phase of this Bora event (except in the 300 m thick layer below 3 km where it had a minimum of 0.96). According to Durran (2003), such a flow accelerates downslope due to the gravity wave overturning and produces a weak return flow above the jet. Using the value $N = 0.015$ s^{-1} and the 8 km wavelength, the internal phase velocity $c_{int} = N\lambda/2\pi \approx 19$ m s^{-1}. The external phase velocity $c_{ext} = \sqrt{g'H} \approx NH$ is 15 m s^{-1} at the ridge and even less on the foothills of the ridge. According to Jiang and Smith's (2003) two-layer model, such a flow is supercritical.

As regards the horizontal structure, Fig. 1 suggests that at first glance the Bora resembles a 2-D phenomenon, but with considerable inhomogeneities perpendicular to the main flow. For example, gaps in the mountain ridge affect the Bora wind speed on the coastline.

Since we are analysing the build-up and decay of Bora gusts we are interested in deviations from local averages and thus local time averages are computed. Some of these time averages are presented in Figs. 3–5. The majority of the study concentrates on vertical cross sections in the W-E direction through the middle of the analysis sub-domain (along $Y = 14$).

There are, on average, two core regions of gusts: at point A on the slope and at point B along the coastline (Fig. 3). (In the analysis sub-domain box of 90 × 30 × 62 points A is at grid point $X = 39$, $Y = 14$, $Z = 2$ and B at 31,14,2).

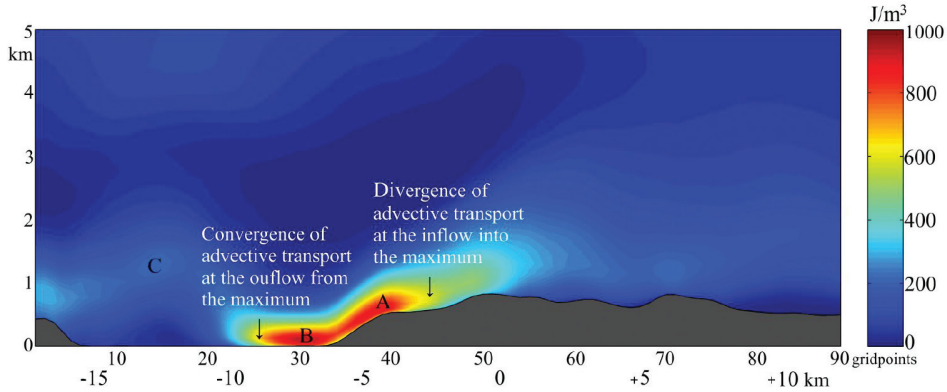

Figure 3. Time average of KE (per unit volume) from 15:10 to 18:00 UTC in a vertical cross-section along $Y = 14$ (W, left to E, right). On the X axis grid points (333 m resolution) and horizontal distance from the top of the mountain ridge (in km) are marked. The average maxima reach around 900 J m^{-3}. The corresponding areas of average divergence of the advective transport of KE on the slope and its convergence over the sea are indicated with arrows. Later in the text, detailed analyses for points A, B and C will be presented and a short comment on conditions on the upwind side of the mountain will be made.

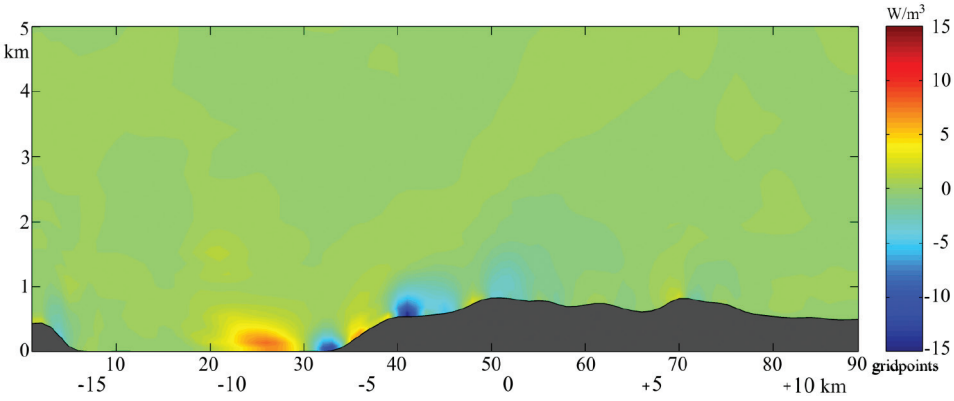

Figure 4. Time average from 15:10 to 18:00 UTC of $Adv = -\nabla \cdot \left(KE\, \vec{v} \right)$ due to the convergence (positive) and divergence (negative) of the advective transport of KE (in W m^{-3}) in the vertical cross section along $Y = 14$.

On the inflow side of a gust, the divergence in a flow becoming faster causes the advection $Adv = -\nabla \cdot \left(KE\, \vec{v} \right)$ effects to be negative – systematically reducing KE, while on the outflow side of a gust in a flow with a decreasing velocity the opposite occurs (see the arrows in Fig. 3); in the centre of a gust the advective contributions are systematically zero (also see Fig. 4).

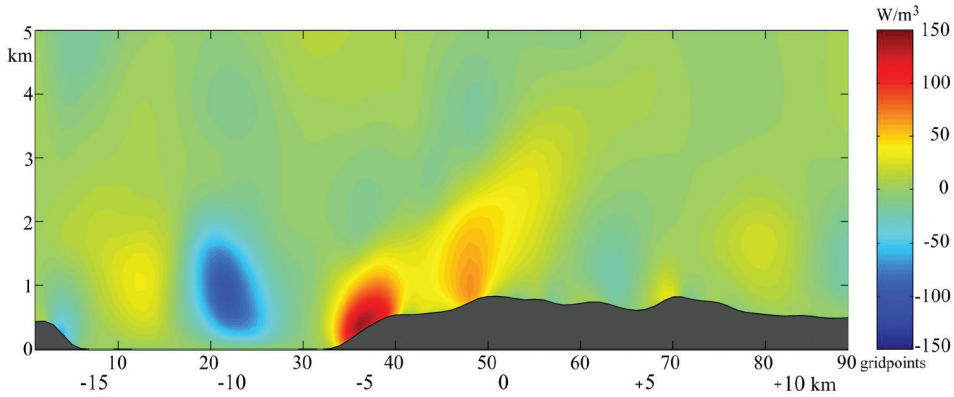

Figure 5. Time average from 15:10 to 18:00 UTC of the gravity force work $\rho\vec{v}\cdot\vec{g} = -\rho wg$ contributions to local changes of *KE* (in W m^{-3}) in the vertical cross section along $Y = 14$.

The average work of gravity force $-\rho wg$ (Fig. 5) also represents vertical motions (negative values indicate upwards motion). The downward motion along the slope is obvious, as is the lifting of the flow in front of the island seen along the left edge of the figure. The most remarkable upward motion is in the region of a jump. The hydraulic jump reaches its maximum amplitude and ascends to its highest level when the gust close to the coastline is the strongest, but almost disappears when the gust elongates along the sea away from the coast. The rotor below intensifies and weakens accordingly.

4.2. Comparison with measurements

In winter 2001–02 the wind was measured on the coastline at Senj 15 m high above the ground during a two-month period with a 1 s time resolution (for details, see Belušić et al., 2004). Data for 8 and 9 December 2001, 48 hours (172 800 s) from these measurements were kindly offered (M. Orlić and M. Pasarić, personal communication, with acknowledgement) to verify the reliability of our simulation with measurements that show the beginning of the Bora in the early hours of 8 December, increasing to a severe stage until around 02 UTC. This severe episode (average speed of almost 20 m s^{-1}) lasted until approximately 17 UTC, when the strength diminished slightly until approximately midnight (average speed of around 15 m s^{-1}). On the next day (not considered by our simulation), the Bora was again severe (again averaging at around 20 m s^{-1}) until 14 UTC when it gradually calmed down. In our simulation, our point (37,8,2) is the closest to Senj. At this model point the gustiness calmed down at around 17:30 UTC but the average speed of the Bora remained severe until the end of the simulation at 18 UTC. We thus compare velocities ($\sqrt{u^2+v^2}$)

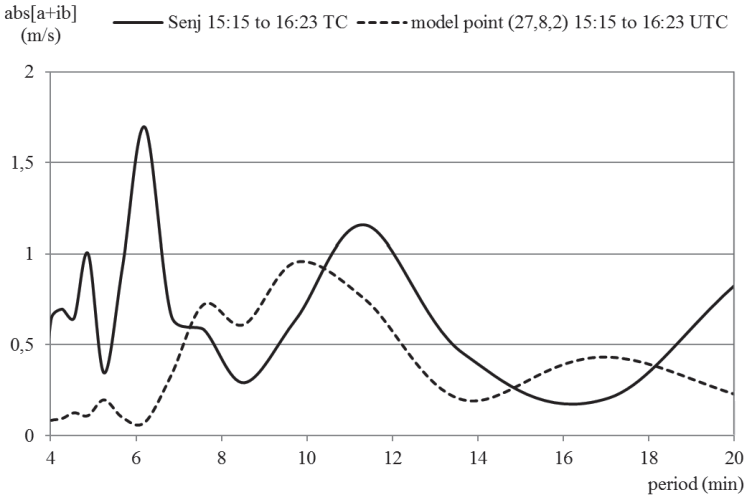

Figure 6. Spectra of wind measured at Senj (M. Orlić and M. Pasarić, personal communication, with acknowledgement, continuous line) and the simulated wind (dashed line) during the 4096 s long time interval from 15:15 to 16:23 UTC. The absolute values of complex numbers, representing pairs of coefficients resulting from FFT of wind velocity data, are shown; 7-time-point moving average smoothing was applied to both. In the measured data there are a lot of signals of short-periods below 4 min, while in the simulation there are none.

only in the time period from 15:15 to 16:23 UTC (the time interval of 2^{12} s = 4096 s) when the Bora was strong in reality and in the simulation. As our simulated data are smoothed with a 7-time-point moving average, we also apply the same smoothing to the measured data. The (smoothed) measured average velocity is 17.7 m s^{-1}, while the average of the simulation in the same time interval is much higher: 30.7 m s^{-1}. On the other hand, the simulated and measured maxima are closer: the (smoothed) measured one is 37.0 m s^{-1} and the simulated one 33.7 m s^{-1}. The measurements represent a 'point', while our simulation represents model volumes (of millions of cubic metres) – that partly explains why simulation overestimates the average velocity, and underestimates of the maxima. The spatial resolution also influences the temporal resolution and the standard deviations of the measured and simulated data are hence quite different: 7.1 m s^{-1} and 1.5 m s^{-1} – although both data sets have the same original temporal resolution of 1 s, and were both smoothed in the same way. This difference may be attributed to the simulation's smoothing in space and in time. As regards periodicity (Fig. 6), the measurements show two main periods: 6.2 min and 11.4 min, while those from the simulation are in between these two: 7.6 min and 9.8 min. Accordingly, in general terms the simulation is relatively successfully in capturing the process in nature, but of course not all of the details.

5. Temporal characteristics

In Bora LLJ there are strong pulsations (Figs. 7 and 9); the strongest gusts develop on model level 2 (over the sea, that is approximately 54 m in height). Gusts and lulls develop with different intensities: in some gusts *KE* reaches only 900 J m^{-3}, while *KE* in the strongest one exceeds 1300 J m^{-3} (Fig. 7). Gusts are developing quasi-periodically with an average period of 8.5 min which roughly corresponds with the 6 to 8 min period measured at Senj as also reported and simulated by Belušić et al. (2009; for the same case with COAMPS and the same spatial resolution). The gusts over the slope precede those over the sea, but their dynamics is beyond pure translation down the slope – which may be seen from the much lower values between the maximum values of two areas of the strongest gusts (red slanted contours) in the Hovmøller diagram (Fig. 9). The phase speed varies from 11 m s^{-1} to 16 m s^{-1} as may be seen from the slants of these contours.

The time courses of *KE* and of the diagnostic terms were closely inspected at points *A* and *B* of the strongest gusts (Fig. 8). Cross-correlations of $KE(t, A)$ at point *A* with *KE* at a down-flow point *B* in some later time $KE(t + \delta t, B)$ reveal not only a delay in the peaks of the gusts, but the relationship of the complete time evolution of *KE* at both points. As seen from these cross-correlations, the time lag of the maximum correlation is $\delta t = 291$ s, which gives an even smaller phase speed down the slope (2664 m / 291 s = 9.2 m s^{-1}). That is considerably less than what was estimated by Belušić et al. (2007) who for shifts along a much longer horizontal distance (of more than 10 km) reported a phase speed of 20 m s^{-1}. For longer distances, our results also show similarly high phase speeds: comparing the times of a gust at upstream point *A* and at point *C* of the hydraulic jump along a horizontal distance of 8 km, we obtain a rough estimate for the phase speed of over 20 m s^{-1}. (Due to chaotic time development at point *C* (Fig. 7) some visual

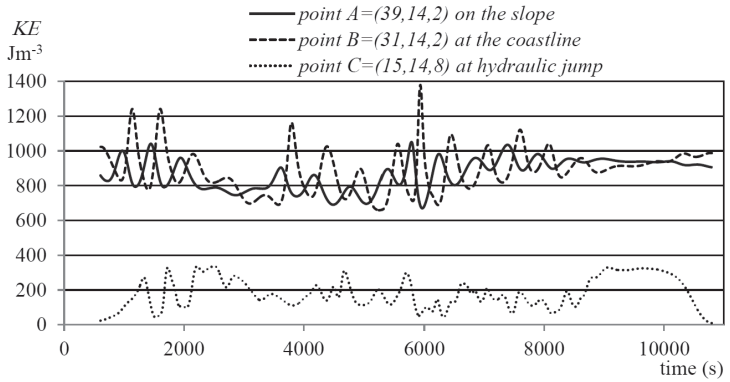

Figure 7. Time courses of *KE* per unit volume at point *A* over the slope, at point *B* close to the coastline, and at point *C* of the hydraulic jump. *A* and *B* are on model level 2 while *C* is on model level 8 (over the sea at an approximate height of 163 m).

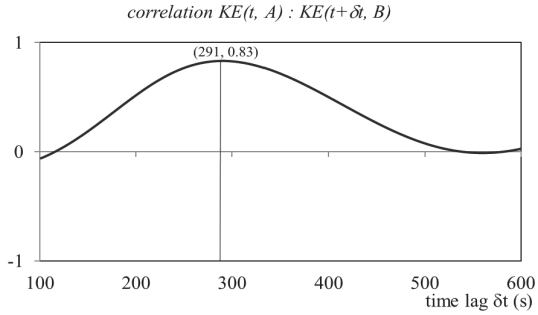

Figure 8. Cross-correlation (non-dimensional, from –1 to +1) of *KE* at point *A* and at point *B* after different time lags δt as a function of that time lag.

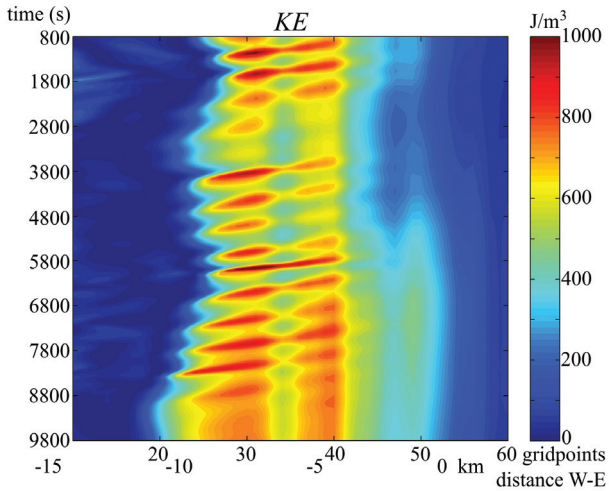

Figure 9. The time-space Hovmøller diagram of *KE* in layer 2 of the model along a W-E direction at $Y = 14$ from (abscise) grid point $X = 10$ to $X = 60$ in time from 800 s to 9800 s (ordinate). One should bear in mind that in the region of a hydraulic jump the jet occasionally weakens and ascends up to model level 8 so its presence is not evident in this diagram.

examination is necessary to properly pair the gusts at *C* with the gusts at *A*). Over the sea alone (from *B* to *C*) the average phase speed is even higher: 26 m s^{-1}.

In a non-stationary Bora *KE*, *Adv*, *Wrk*, and *Turb* oscillate in the two areas of maximum gusts (Figs. 10 and 12). At point *A* over the slope (Fig. 10), *KE* typically oscillates roughly by ±2 W m^{-3}, while before and after the strongest gust (at approximately 6000 s) it reaches approximately ±5 W m^{-3}. The contribution of advection effects *Adv* is strongly oscillating. The time average of *Adv* is not exactly zero, meaning that point *A* is not exactly the average location of the gusts, but is slightly in the lee of it (only by pure chance could a grid-point be at ex-

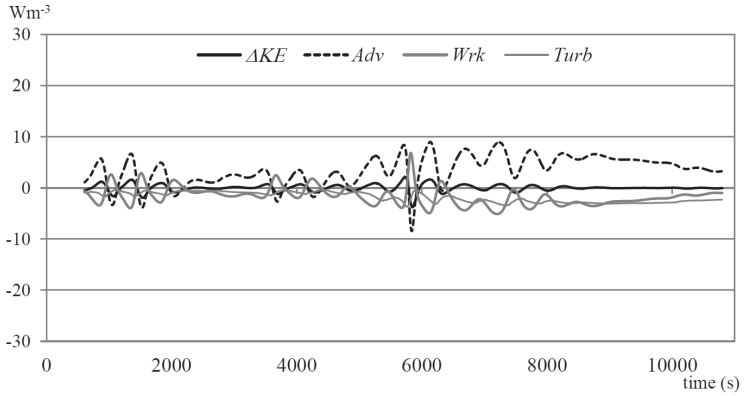

Figure 10. Time courses of Δ*KE*, and of the contributions of *Adv*, *Wrk* and *Turb* to it at point *A* of the gusts on the slope.

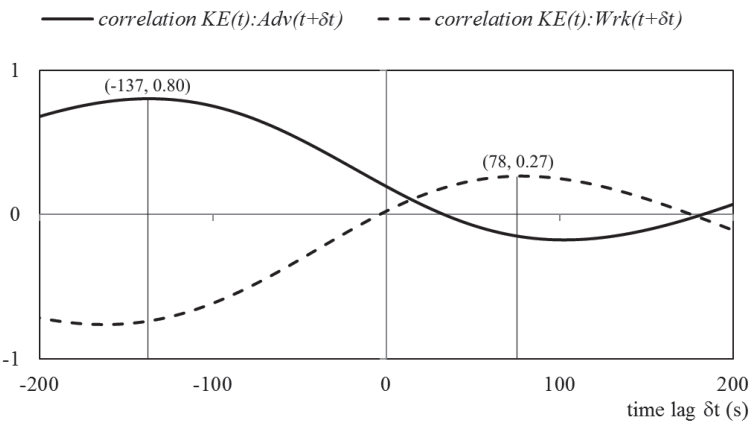

Figure 11. Cross-correlations at point *A* (non-dimensional, from –1 to +1) between the 2 h long time courses of *Adv* (t_1, t_2) and *Wrk* (t_1, t_2) and *KE*($t_1+\delta t$, $t_2+\delta t$) at the same point for different time lags δt from δt = –200 s to δt = +200 s as a function of that time lag.

actly the average location of gusts). The highest value of *Adv* reaches 9 W m^{-3} shortly before the strongest gust and, immediately afterwards, it drops to –9 W m^{-3}. The amplitudes of *Wrk* are smaller than those of *Adv*. *Turb* is negative all the time. The gustiness slowly dies out after t = 9000 s (after 17:30 UTC). Fig. 10 shows that phase of *Adv* is 137 s ≈ 2.3 min ahead of *KE* at point *A* on the slope while *Wrk* is 78 s = 1.3 min after *KE*; so *Wrk* and *Adv* are approximately in an opposite phase.

At point *B* over the sea, close to the coastline, Δ*KE* typically oscillates by ±5 W m^{-3} (Fig. 12), while before and after the strongest gust at approximately

6000 s it reaches approximately ±10 W m^{-3}. The contribution of advection effects *Adv* is strongly oscillating. The highest values of *Adv* in general reach some ±10 W m^{-3}, with +30 W m^{-3} shortly before the strongest gust and –25 W m^{-3} after it. (Also here the non-zero time average of *Adv* means that point *B* is also not exactly the average location of the gusts, but slightly upwind of it.) *Wrk* is mainly positive here with amplitudes that are again smaller than those of *Adv*. *Turb* is small, and occasionally positive. Fig. 13 shows that the phase of *Adv* is 105 s = 1.75 min ahead of *KE* at point *B* on the slope while *Wrk* again is 73 s = 1.2 min after *KE*.

The Hovmøller diagram of *Adv* (Fig. 14a) clearly shows that the advection is not continuous along model layer 2: the positive values of *Adv* are spatially interrupted by strong negative ones. There are clear gaps during the whole episode on the upper part of the slope (the vertical blue strip around $X = 41$) and

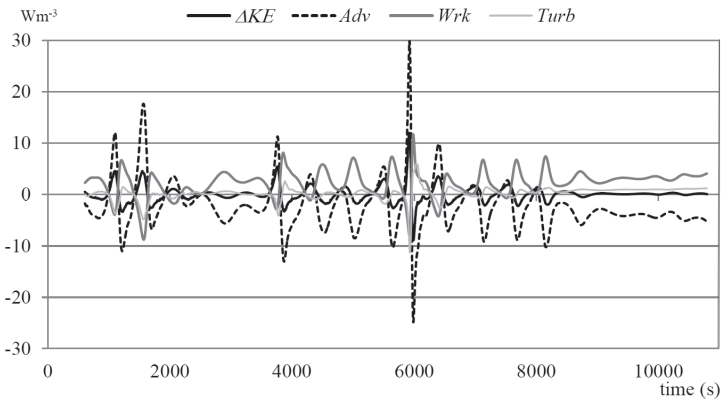

Figure 12. The same as Fig. 10, but at point *B* of gusts on the coastline.

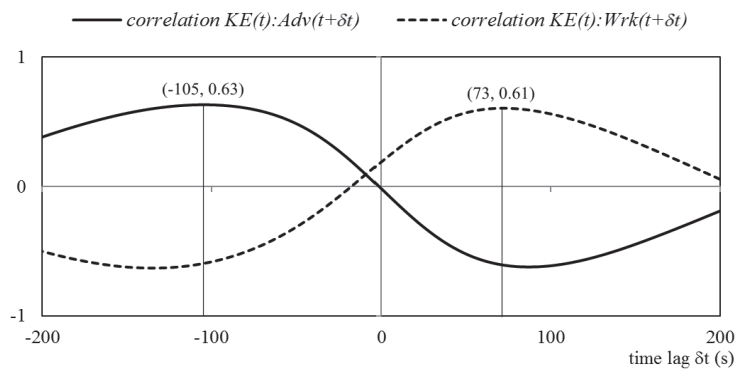

Figure 13. The same as Fig. 11, but at point *B* of gusts on the coastline.

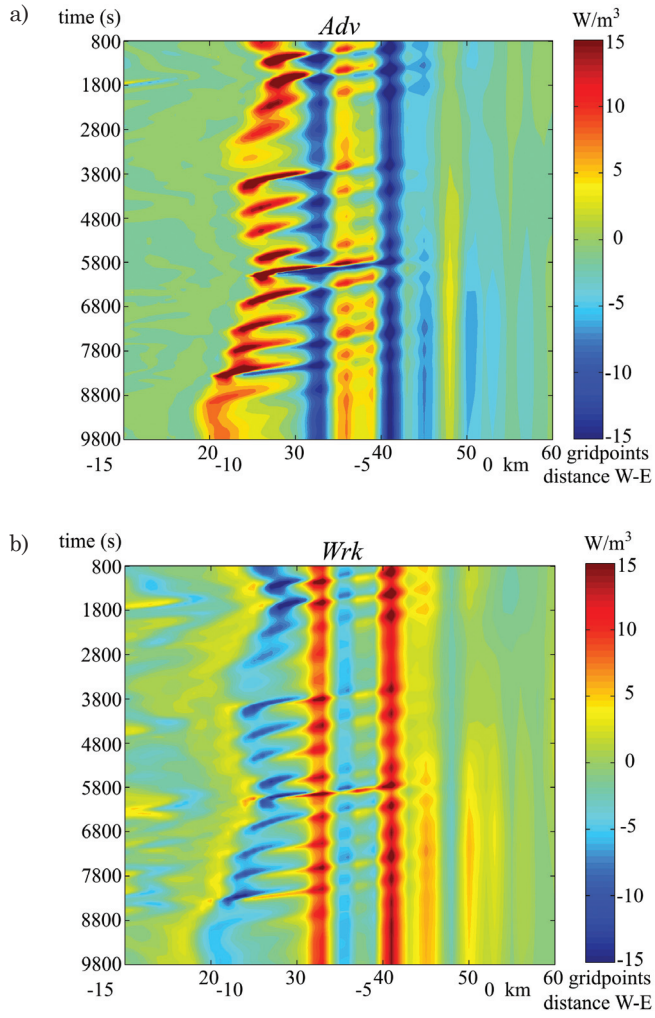

Figure 14. The same as Fig. 7, but for *Adv* (*a*) and of *Wrk* (*b*).

between the two regions of maximum gusts (the vertical blue strip between $X = 31$ to $X = 34$). *Wrk* (Fig. 14b) shows the opposite structure: where *Adv* is positive *Wrk* is negative, and vice versa. This means that *Wrk* effectively replaces *Adv* in transporting *KE* during specific phases of the evolution of gusts.

On the upwind side of the main mountain ridge where the Bora jet forms, processes are quite stationary and do not exhibit any significant periodic behaviour. On the lee side of the gusts in the region of the hydraulic jump, around point $C(15,14,8)$, ***KE*** and all diagnostic terms are much smaller than in the regions of

the gusts, and the development there is less periodic, it is relatively chaotic. *Adv* is small there, *Wrk* is approximately ten times bigger, but mostly positive (tending to increase *KE)*. As changes ΔKE are small as well, it is *Turb* that approximately balances the positive *Wrk* – i.e. it is strongly dissipating *KE*.

Local fluctuations of *Adv* are caused by spatial and temporal velocity differences, while *Wrk* may fluctuate due to a changing velocity or due to a changing pressure gradient. (Perhaps it is worth repeating that *Wrk* is what remains after hydrostatic vertical pressure gradient force cancels with gravity.) The part Wrk_y caused by velocity normal to the main flow is almost negligible in comparison to Wrk_x, at both points *A* and *B*. On the slope (point *A*) Wrk_{znh} and Wrk_x have comparable magnitudes, but opposite signs: Wrk_{znh} oscillates around –20 W m^{-3} and Wrk_x around +20 W m^{-3}. The resulting total *Wrk* is thus small over the slope and oscillates by some ±5 W m^{-3} around zero and reaches +10 W m^{-3} at the strongest gust. At point *B* the *Wrk* fluctuations are almost twice as large: approximately ±8 W m^{-3} and reach +15 W m^{-3} during the main gust; as Wrk_{znh} is much smaller, mainly due to Wrk_x.

The Bora wind in LLJ does not change direction – it is westwards and downwards for all of the time. Thus one could speculate in advance that mainly pressure gradient fluctuations cause positive and negative *Wrk* fluctuations. To test this, we split the velocity and pressure gradient into their local time averages denoted by $\langle\ \rangle$, and the departures from these denoted by ': for example $u = \langle u \rangle + u'$ and $\frac{\partial p}{\partial x} = \left\langle \frac{\partial p}{\partial x} \right\rangle + \frac{\partial p'}{\partial x}$, and $w = \langle w \rangle + w'$ and $\frac{\partial p_{nh}}{\partial x} = \left\langle \frac{\partial p_{nh}}{\partial x} \right\rangle + \frac{\partial p_{nh}'}{\partial x}$.

At point *B*, Wrk_x is well represented by u and $\frac{\partial p}{\partial x}$ (the term $u\frac{\partial p}{\partial z}\frac{\partial z}{\partial x}$ may be neglected here as the model levels are quite horizontal over the sea). So we consider $-u\frac{\partial p}{\partial x} = -\langle u \rangle \left\langle \frac{\partial p}{\partial x} \right\rangle - \langle u \rangle \frac{\partial p'}{\partial x} - u' \left\langle \frac{\partial p}{\partial x} \right\rangle - u' \frac{\partial p'}{\partial x}$. The first term on the RHS is constant since it is a product of two averages, while the other three vary in time. It is evident from Fig. 15 that the time changes of horizontal pressure gradient $\frac{\partial p'}{\partial x}$ really cause most of the *Wrk* fluctuations along the horizontal direction. $-\langle u \rangle \frac{\partial p'}{\partial x}$ together with the constant term $-\langle u \rangle \left\langle \frac{\partial p}{\partial x} \right\rangle$ almost entirely cover the total fluctuations of work along the horizontal; the other two terms are much smaller and their contributions are minor.

On the other hand, the departures of vertical velocity w' from its time average at point *B* are the almost exclusive cause of (much smaller) temporal variations in work effects along the vertical: $-w' \left\langle \frac{\partial p_{nh}}{\partial z} \right\rangle$ represents almost the total work done along the vertical direction. (Correlation coefficient R between the time courses of *Wrk* and of w' is +0.9999!)

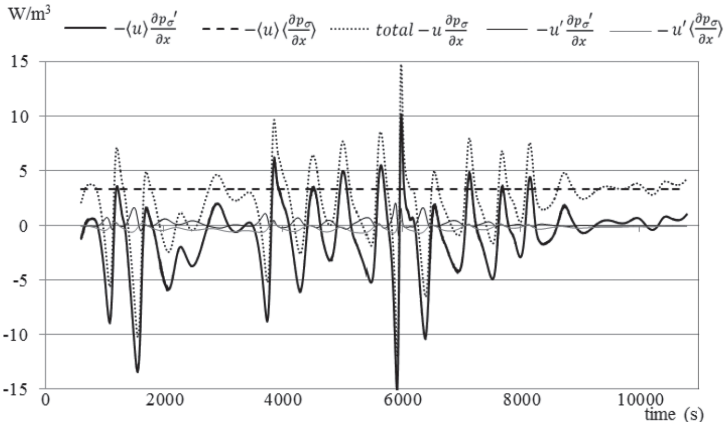

Figure 15. Contributions of different combinations of averages of the u-component of wind velocity and of the pressure gradient along the x-direction and the departures from those averages to the work of forces along the *x*-direction at point *B* on the coastline.

6. Relation between advective effects and effects of work

Data from our simulation show that the Wrk amplitudes are generally smaller than those of Adv and that both time courses are in approximately the opposite phase: when and where one is positive, the other is negative and vice versa. The detailed time courses for the strongest gust clearly confirm this (Figs. 16a and b).

These characteristics of *Wrk* versus *Adv* in the simulated Bora may be compared to an idealised stationary adiabatic flow without phase changes, with negligible friction and energy dissipation. Such a flow obeys the Bernoulli-Bjerknes equation $\frac{d}{dt}\left(\frac{u^2}{2}+gz+c_pT\right)=0$ (e.g. Bjerknes et al., 1933, p. 173). A mass moving in such a flow keeps its total energy along some distance down the flow: $u\delta u+g\delta z+c_p\delta T=0$ and, as in adiabatic flow $c_p\delta T=\delta p/\rho$, also $\rho u\delta u+\rho g\delta z+\delta p=0$. By multiplying that equation by u one obtains $\rho u^2\delta u+\rho ug\delta z+u\delta p=0$. For horizontal flow ($\delta z=0$) the balance $-u\delta p=\rho u^2\delta u$ remains. The left-hand-side $-u\delta p$ is proportional to Wrk_{hor} and the right-hand-side $\rho u^2\delta u$ is proportional to $-\frac{2}{3}(Adv+\frac{c_v}{c_p}\frac{KE}{p}Wrk_{hor})$. [As $-\delta\left(\rho uu^2/2\right)=$-
$=-\frac{3}{2}\rho u^2\delta u-\delta\rho u^3/2$ and as in adiabatic flow $\frac{\delta\rho}{\rho}=\frac{c_v}{c_p}\frac{\delta p}{p}$, it follows $-\delta\left(\rho uu^2/2\right)=$
$=-\frac{3}{2}\rho u^2\delta u-\frac{u^3}{2}\frac{c_v}{c_p}\frac{\rho}{p}\delta p.$]

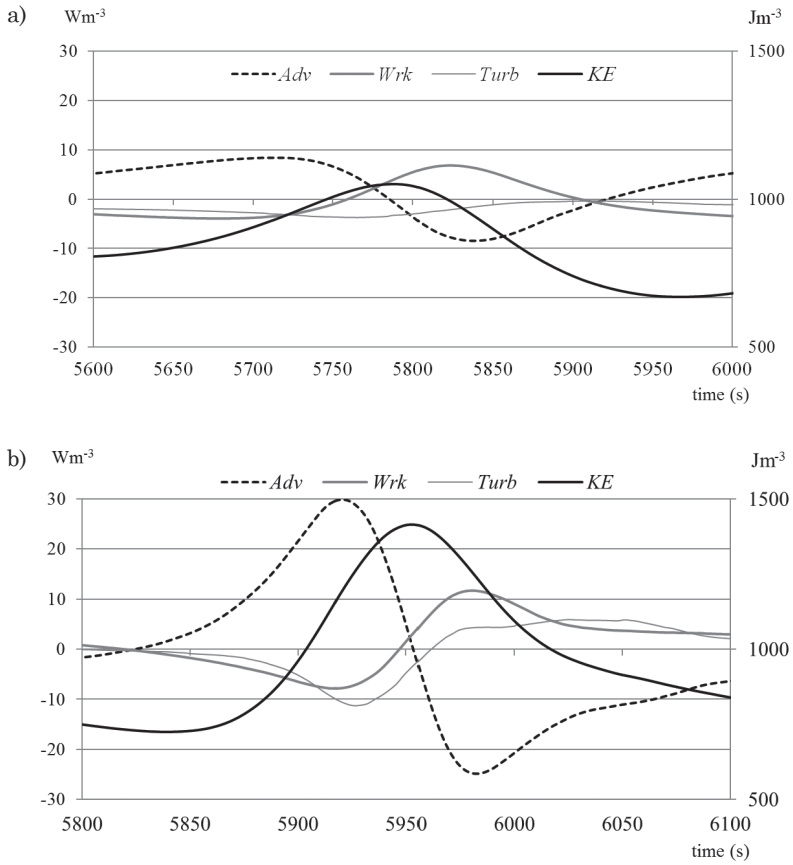

Figure 16. Details of time courses of Wrk, Adv, $Turb$ and KE for the strongest gust (*a*) at point A over the slope and (*b*) at point B over the sea close to the coastline.

So for such an idealised flow $Wrk_{hor}\left(1-\frac{2c_v}{3c_p}\frac{KE}{p}\right)=-\frac{2}{3}Adv$. The second term $\frac{2c_v}{3c_p}\frac{KE}{p}$ in parenthesis, describing compressibility effects, is small: $\frac{2c_v}{3c_p}\frac{KE}{p}\sim 10^{-2}-10^{-3}$, thus:

$$Wrk_{hor}\approx-\frac{2}{3}Adv\,.$$

In a flow down the slope the term $g\delta z$ should also be considered. But because we only consider the work due to the non-hydrostatic vertical pressure gradient along the vertical direction (the hydrostatic part cancels with gravity), the same

basic relation between Wrk and Adv should also hold for the idealised flow down the slope.

The Bora flow is relatively adiabatic, in many cases it is without phase changes (at least in the lee of a mountain), but it is not stationary, not completely frictionless and not without dissipation. So the time courses Wrk and Adv in Bora are not necessarily exactly in opposite phases and Wrk is not necessarily everywhere and continuously smaller than Adv. Still, the simulation data show that Wrk is approximately in the opposite phase to Adv and is generally smaller than Adv – as for the considered idealised flow: at point A the average value (in 2.5 hours of simulation from t = 800 s to t = 9800 s) of Wrk in comparison to Adv is –0.553 and at point B it is –0.602; close to the –2/3 = –0.667 in the idealised flow.

The above consideration at least partly explains the interplay of Wrk and Adv down the slope: the strongly expressed vertical belts of an opposite sign in the Hovmøller diagrams for Wrk and Adv (Figs. 14a and b).

7. Conclusions

The transport equation for kinetic energy (*KE*) was used to diagnose the contributions of different processes to the local build up and decay of gusts and lulls in the Bora flow. The terms of the equation were calculated for a Bora case of 8 December 2001 in every time step during three hours of Bora WRF simulation results in a 333 m resolution. The analysis focused on the time and spatial variability of these terms, and how they are correlated with the velocity magnitude at some distinct locations in the Bora jet.

It was found that, besides the advection, the work done by the horizontal pressure gradient force, the non-hydrostatic vertical pressure gradient force, turbulent diffusion and dissipation are the processes that govern the spatial and temporal evolution of the *KE*, associated with periodic wind speed changes – pulsations.

The simulation reveals two regions of the strongest gusts: one over the mountain, roughly where the terrain declines into its steepest, final slope down to the sea, and the second at the bottom over the sea, roughly one kilometre from the coastline. It was also found that the speed with which the gusts propagate down the slope is not equal to the average wind speed between the two locations, but about twice as slow. Moreover, a Hovmøller diagram showed that there is a certain degree of discontinuity in the gusts and lulls translation, indicating that mechanisms beyond advection are responsible for their propagation.

The advection and the work of the pressure gradient force effects are roughly in an opposite phase: advection effects reach their maxima roughly 2 min

before the *KE* peaking at both locations of maximum gusts, while the effects of the work done by forces reach their maxima when *KE* already diminishes. The Bora flow in the analysed case was also found to closely resemble a quasi-stationary adiabatic flow: the ratio between the effects of the work done by the pressure forces and the advective effects at the two points of maximum gusts are on average –1.66/3 and –1.81/3 – quite close to the theoretical –2/3 for the idealised flow. The turbulent diffusion and dissipation of *KE*, being the smallest of all effects, were diagnosed from the sum of the local time changes of *KE* and the sum of the advection and work of forces terms.

Acknowledgements – The research was completed within the scope of a research programme under Grant P1-0188 from the Slovenian Research Agency. The use of wind measurement data in Senj by our Croatian colleagues M. Orlić, M. Pasarić and D. Belušić is acknowledged for verification of the simulation results. The authors appreciate the initial discussion on the research approach with B. Grisogono, D. Belušić and Ž. Večenaj. The suggestions of the two reviewers helped to fundamentally improve the paper. J. Rakovec and R. Žabkar were employed part-time with the Slovenian Centre of Excellence for Space Sciences and Technologies SPACE-SI, being an operation that is partly financed by the European Union, the European Regional Development Fund and the Ministry of Higher Education, Science and Technology of the Republic of Slovenia.

References

AMS Glossary, http://glossary.ametsoc.org/wiki/Bora

Baklanov, A. and Grisogono, B. (2007): Atmospheric boundary layers: Nature, theory and applications to environmental modelling and security, *Boundary Layer Meteorol.* **125**, 157–160, DOI: 10.1007/s10546-007-9217-2.

Belušić, D., Pasarić, M. and Orlić, M. (2004): Quasi-periodic bora gusts related to the structure of the troposphere. *Quart. J. Roy. Meteor. Soc.*, **130**, 1103–1121, DOI: 10.1256/qj.03.53.

Belušić D., Žagar, M. and Grisogono, B. (2007): Numerical simulation of pulsations in the bora wind, *Quart. J. Roy. Meteor. Soc.*, **133**, 1371–1388, DOI: 10.1002/qj.129.

Bjerknes, V., Bjerknes, J., Solberg, H. and Bergeron, T. (1936): *Physikalische Hydrodynamik mit Anwendung auf die Dynamische Meteorologie*. Berlin, Springer, xvii+797 s.

Durran, D. R. (2003): Lee waves and mountain waves, in *Encyclopedia of the Atmospheric Sciences,* edited by Holton, J. R., Curry, J. A. and Pyle, J., Academic Press, 1161–1169.

Gohm, A., Mayr, G. J., Fix, A. and Giez, A. (2008): On the onset of bora and the formation of rotors and jumps near a mountain gap, *Quart. J. Roy. Meteor. Soc.*, **134**, 21–46, DOI: 10.1002/qj.206.

Grisogono, B. and Belušić, D. (2009): A review of recent advances in understanding the meso- and microscale properties of the severe bora wind, *Tellus*, **61A**, 1–16, DOI: 10.1111/j.1600-0870.2008.00369.x.

Jiang, Q. and Smith, R. B. (2003): Gravity wave breaking in two-layer hydrostatic flow, *J. Atmos. Sci.*, **60**, 1159–1172, DOI: 10.1175/1520-0469(2003)060<1159:GWBITH>2.0.CO;2.

Klemp, J. B. and Durran, D. (1987): Numerical modelling of bora winds, *Meteorol. Atmos. Phys.*, **36**, 215–227. DOI: 10.1007/BF01045150.

Petkovšek, Z. (1982): Gravity waves and bora gusts, *Ann. Meteorol. (N.F.)*, **19**, 108–110.

Petkovšek, Z. (1987): Main bora gusts – a model explanation, *Geofizika*, **4**, 41–50, available at http://geofizika-journal.gfz.hr/Vol_04/Petkovsek.pdf

Poulos, G. S., Bossert, J. E., McKee, T. B. and Pielke Sr., R. A. (2007): The interaction of katabatic flow and mountain waves. Part II: Case study analysis and conceptual model, *J. Atmos. Sci.*, **64**, 1857–1879, DOI: 10.1175/JAS3926.1

Rakovec, J. (1987): Preliminary report on spectral characteristics of bora on the island of Rab, *Geofizika*, **4**, 35–40, available at http://geofizika-journal.gfz.hr/Vol_04/Rakovec.pdf

Rotach, M. W. and Zardi, D. (2007): On the boundary-layer structure over highly complex terrain: Key findings from MAP, *Quart. J. Roy. Meteor. Soc.*, **133**, 937–948, DOI: 10.1002/qj.71.

Skamarock, W. C., Klemp, J. B., Dudhia, J., Gill, D. O., Barker, D. M., Duda, M., Huang, X.-Y., Wang, W. and Powers, J. G. (2008): A description of the advanced research WRF version 3. *NCAR Technical note NCAR/TN-475+STR*, 113 pp, available online at www2.mmm.ucar.edu/wrf/users/docs/arw_v3.pdf

Smith, R. B. (1987): Aerial observations of the Yugoslavian bora, *J. Atmos. Sci.*, **44**, 269–297, DOI: 10.1175/1520-0469(1987)044<0269:AOOTYB>2.0.CO;2.

Smith, R. B. and Sun, J. (1987): Generalized hydraulic solutions pertaining to severe downslope winds, *J. Atmos. Sci.*, **44**, 2934–2939, DOI: 10.1175/1520-0469(1987)044<2934:GHSPTS>2.0.CO;2.

Smith, R. B., Doyle, J. D., Jiang, Q. and Smith, S. A. (2007): Alpine gravity waves: Lessons from MAP regarding mountain wave generation and breaking, *Quart. J. Roy. Meteor. Soc.*, **133**, 917–936, DOI: 10.1002/qj.103.

Van Migheim, J. (1973): *Atmospheric energetics*. Oxford University Press, xi+306 pp.

Yoshino, M. M. (editor) (1976): *Local wind bora*. University of Tokyo Press, Tokyo, 289 pp.

SAŽETAK

Utjecaj advekcije i rada sila na mahovitost bure

Jože Rakovec, Rahela Žabkar i Mark Žagar

Lokalne promjene vjetra u buri istražene su u slučaju od 8. prosinca 2001. koji je bio simuliran WRF/ARF modelom s horizontalnom rezolucijom od 333 m i sa svim relevantnim modelskim varijablama arhiviranim tijekom 3-satnog vremenskog intervala s vremenskom rezolucijom od 1 s. Duž odabranog presjeka paralelnog s burom nađene su dvije lokacije u navjetrini Dinarida s jakim udarima – jedna na obronku planine i druga iznad mora blizu obale, dok je između njih vjetar znatno slabiji. U promatranom trosatnom intervalu razvilo se oko 16 do 18 udara vjetra s prosječnim periodom od približno 8,5 minuta. Advektivni transport kinetičke energije (*KE*), rad neuravnoteženog dijela sile gradijenta tlaka te difuzija i disipacija *KE* uzrokuju lokalnu promjenu ΔKE, i njihove kvazi-periodičke fluktuacije vode do pojave udara i zatišja. Rezultati numeričke simulacije omogućavaju procjenu doprinosa advekcije, rada sila te učinaka turbulencije i disipacije. Advekcijski doprinosi lokalnim promjenama su više ili manje u fazi s ΔKE i ispred faze *KE*, a doprinosi rada su općenito manji i u suprotnoj fazi. To znači da advekcija i rad općenito djeluju suprotno. Učinci advekcije i rada nisu prostorno homogeni, tj. oni prestaju ili čak mijenjaju predznak između dvije lokacije najjačih udara. Stoga nema kontinuiranog pomaka *KE* od više prema nižoj lokaciji koji bi bio uzrokovan bilo kojim od ova dva učinka: njihovi se doprinosi međusobno izmjenjuju niz obronak.

Ključne riječi: mahovitost bure, interna dinamika strujanja, WRF-ARW model

Corresponding author's address: Jože Rakovec, University of Ljubljana, Faculty of Mathematics and Physics, Chair of Meteorology, Jadranska 19, and Slovenian Centre of Excellence for Space Sciences and Technologies – SI, 1000 Ljubljana, Slovenia; e-mail: joze.rakovec@fmf.uni-lj.si

Appendix A

The balance equation for *KE* (1) describes the local tendency of the *KE* per unit volume: $\frac{\partial KE}{\partial t} = -\nabla \cdot \left(KE\vec{v}\right) - \vec{v} \cdot \nabla p + \rho\vec{v} \cdot \vec{g} + \rho\vec{v} \cdot \vec{f}$.

On the RHS, we find:

$-\nabla \cdot \left(KE\vec{v}\right)$, standing for the convergence of the advective transport of *KE*; this is not the source or sink of KE – it only spatially redistributes it; when and where this advective effect is positive it contributes to a local increase in *KE*.

$-\vec{v} \cdot \nabla p$ the work done by the pressure gradient force (power per unit volume); a source or a sink of KE, locally increasing where and when the velocity is directed towards the decreasing pressure and reducing *KE* if the velocity points towards increasing pressure.

$\rho\vec{v} \cdot \vec{g} = -\rho wg$, the work done by, or against, the gravity force (again power per unit volume); the source or sink of *KE* – positive for downwards motion.

$\rho\vec{v} \cdot \vec{f}$, turbulent diffusion and dissipation (in numerical models also numerical diffusion). The dissipation part of it is a sink of KE and is systematically negative. Turbulent diffusion has a damping effect on the local extremes. Thus, the diffusion effects can also be positive at locations of strong local minima and may prevail over dissipation to make the total effects locally positive. Because turbulence and dissipation are typically parameterised in numerical models, their magnitudes in models also depend on the parameterisation used. Boundary layers and turbulence in complex terrain are poorly understood even today (Grisogono and Belušić, 2009; Baklanov and Grisogono, 2009; Rotach and Zardi, 2007) and consequently any parameterisation is necessarily merely an approximation. The choice of parameterisation thus in particular affects the overall wave-turbulence interaction (e.g. Smith et al., 2007; Gohm et al., 2008). In our diagnostic approach, this term will not be computed explicitly, but diagnosed from the values of all the other terms:

$$Turb \equiv \rho\vec{v} \cdot \vec{f} = \frac{\partial\left(KE\right)}{\partial t} + \nabla \cdot \left(KE\vec{v}\right) + \vec{v} \cdot \nabla p - \rho\vec{v} \cdot \vec{g}.$$

The splitting of processes and variables into an appropriate background state and the departures from it is a well-known approach. In most cases, density is split into the horizontally homogeneous $\rho_0(z)$ that only decreases with height, and its perturbation. The basic pressure $p_0(z)$ then follows $\frac{\partial p_0}{\partial z} = -\rho_0 g$. Often wind is also split into a basic wind $U_0(z)$ that only increases in a vertical direction, and perturbations. Since in our case the wind is very weak on the windward side in comparison to the velocity of the Bora jet (see Figs. 1 and 2), it is much more convenient to split it locally into local time averages $\langle u \rangle (x,y,z)$ and depar-

tures $u'(x,y,z,t)$, and similarly for other variables: $\langle\rho\rangle(x,y,z)$ and $\rho(x,y,z,t)$ etc. As regards pressure, in our case it is more convenient to split it locally into the hydrostatic part p_h that varies in space and in time, and the departures p_{nh}: $p(x,y,z,t) = p_h(x,y,z,t) + p_{nh}(x,y,z,t)$. With such a splitting, for example, buoyancy conveniently no longer appears as a separate term in the vertical equation of motion (see Appendix B). In Section 6, where the effects of the work done by the pressure gradient force are investigated in detail, we will further divide these into various combinations of their local time averages and departures from these: e.g. $\langle u\rangle\left\langle\frac{\partial p}{\partial x}\right\rangle$, $u'\left\langle\frac{\partial p}{\partial x}\right\rangle$, $\langle u\rangle\frac{\partial p'}{\partial x}$ and $u'\left\langle\frac{\partial p'}{\partial x}\right\rangle$ along both horizontal and vertical directions.

After splitting the pressure into the hydrostatic and non-hydrostatic parts in Eq. (1), the gravity effects completely cancel the effects of the hydrostatic part of the vertical pressure gradient force. Only the work done by the non-hydrostatic part remains from the two terms $-\vec{v}\cdot\nabla p + \rho\vec{v}\cdot\vec{g} = -w\frac{\partial p_{nh}}{\partial z} - \vec{v}_h\cdot\nabla_h p$. In such a simplified form of Eq. (1), advection $Adv = -\nabla\cdot(KE\vec{v})$, the work of the remaining pressure gradient force $Wrk = \left(-w\frac{\partial p_{nh}}{\partial z} - \vec{v}_h\cdot\nabla_h p\right)$ and the diffusion and dissipation effects $Turb = \rho\vec{v}\cdot\vec{f}$ contribute to the local changes of *KE*.

Appendix B

This is to show that $-w\,\partial p_{nh}/\partial z$ properly considers all work done along the vertical direction, including buoyancy.

In our paper the pressure is split into hydrostatic and non-hydrostatic parts: $p = p_h + p_{nh}$, where $\partial p_h/\partial z = -\rho g$ (with the local value ρ that varies in space and time). On the other hand, the splitting that is normally undertaken using a constant density ρ_0 and $\partial p_0/\partial z = -\rho_0 g$ would lead to an explicit buoyancy term.

No matter how the division of pressure is done, the vertical pressure gradient ∂p/∂z must be the same, and both expressions can be worked out as follows:

$$\partial p_h/\partial z + \partial p_{nh}/\partial z = \partial p_0/\partial z + \partial(p - p_0)/\partial z,$$

$$-\rho g + \frac{\partial p_{nh}}{\partial z} = -\rho_0 g + \frac{\partial(p - p_0)}{\partial z}.$$

It is evident from this expression, without any approximation, that $\partial p_{nh}/\partial z$ includes both the pressure perturbation term $\partial\left(p-p_0\right)/\partial z$, and the density perturbation buoyancy term $\left(\rho-\rho_0\right)g$:

$$\frac{\partial p_{nh}}{\partial z}=\left(\rho-\rho_0\right)g+\partial\left(p-p_0\right)/\partial z.$$

So $-w\frac{\partial p_{nh}}{\partial z}$ does consider the work due to departures of the vertical pressure gradient from $\frac{\partial p_0}{\partial z}=-\rho_0 g$ and the work of buoyancy.